2.H:3.A *Nuclear Physics* A154 (1970) 499—512; © *North-Holland Publishing Co., Amsterdam*

REORIENTATION MEASUREMENTS IN ^{116}Sn AND ^{124}Sn

A. M. KLEINFELD †, RENATA COVELLO-MORO ††, H. OGATA †††,
G. G. SEAMAN ‡, S. G. STEADMAN ‡‡ and J. DE BOER ‡‡‡
Department of Physics, Rutgers-the State University, New Brunswick, New Jersey *,

Received 25 June 1970

Abstract: The first 2^+ states of ^{116}Sn and ^{124}Sn have been studied by observing the γ-ray decay to the ground states, following Coulomb excitation with backscattered ^{4}He, ^{16}O and ^{32}S ions. The static electric quadrupole moment Q_{2+} of the 2^+ states and the reduced electric transition probability $B(\mathrm{E2}, 0^+ \rightarrow 2^+)$ were obtained by interpreting the results in terms of the reorientation effect. The values of Q_{2+} found are $+0.09 \pm 0.13$ b for ^{116}Sn and -0.24 ± 0.15 b for ^{124}Sn. The measured $B(\mathrm{E2}, 0^+ \rightarrow 2^+)$ values are $0.22 \pm 0.01\ e^2 \cdot \mathrm{b}^2$ for ^{116}Sn and $0.19 \pm 0.01\ e^2 \cdot \mathrm{b}^2$ for ^{124}Sn.

E COULOMB EXCITATION ^{116,124}Sn, (^{4}He, ^{4}He$'\gamma$), (^{16}O, ^{16}O$'\gamma$), (^{32}S, ^{32}S$'\gamma$), E = 2–2.5 MeV/nucleon; measured $\sigma(E_\alpha, E\gamma, \theta\gamma)$, $\sigma(E(^{16}\mathrm{O}'), E\gamma, \theta\gamma)$, $\sigma(E(^{32}\mathrm{S}'), E\gamma, \theta\gamma)$. ^{116,124}Sn levels deduced B(E2), Q.

1. Introduction

Recently, there has been a great deal of interest in medium-weight vibrational nuclei, motivated to a large extent by the measurements of the static quadrupole moments of the first 2^+ states (Q_{2+}) of several even nuclei [1]). Most nuclear models appropriate to nuclei with vibrational spectra fail to reproduce the large values of Q_{2+} measured in these experiments. Previous experimental studies have been made on the even nuclei with charge numbers a few units away from the closed proton shell $Z = 50$. The tin ($Z = 50$) isotopes are expected to be nearly spherical and should therefore have particularly small quadrupole moments [2,3]).

The experimental technique used was to measure the γ-ray spectrum in coincidence with the backscattered projectiles (^{4}He, ^{16}O and ^{32}S ions). The measured excitation probabilities for each projectile have been interpreted in terms of the reorientation effect.

† Present address: Institut für Kernphysik, Universität Köln, Köln, Germany.
†† Present address: Istituto di Fisica Superiore, Università di Napoli, Napoli, Italy.
††† On leave from Kyoto University, Japan.
‡ Present address: Kansas State University, Manhattan, Kansas.
‡‡ Present address: Physikalisches Institut, Universität Erlangen-Nürnberg, Erlangen, Germany.
‡‡‡ Present address: Sektion Physik, Universität München, München, Germany.
* Supported in part by the National Science Foundation.

Sect. 2 consists of a brief discussion of the theory. The apparatus and the experimental procedure are described in sect. 3, and the results are presented in sect. 4. The last section contains the analysis of the results in terms of the reorientation effect.

2. Theory

2.1. MEASURED QUANTITY

The ratio R measured in this experiment is the number of de-excitation γ-rays from the 2^+ state to the ground state that are in coincidence with the backscattered particles, divided by the number of backscattered particles. In terms of the differential cross sections $d\sigma$ for exciting level i, R is given by

$$R = \frac{\sum_{i=2}^{N_{max}} f_i \, d\sigma_i}{\sum_{i=1}^{N_{max}} d\sigma_i} . \tag{1}$$

The sum in the denominator includes the ground state (index $i = 1$) while the sum in the numerator is taken from the first 2^+ state ($i = 2$) to an appropriate maximum value N_{max}. The quantities f_i are the fractions of decays of the ith level proceeding via the first 2^+ state.

The excitation probability P for exciting the first 2^+ state may be written as

$$P = \frac{d\sigma_2}{\sum_{i=1}^{N_{max}} d\sigma_i} . \tag{2}$$

For the experiments described here, the cross sections to higher levels ($i \geqq 3$) are so small that $R \approx P$. We will now consider two ways of calculating R (or P), namely by perturbation theory and by numerical integration with a computer.

2.2. PERTURBATION THEORY

The results of perturbation theory are briefly discussed because they offer a convenient way of describing the important aspects of the experiment. The perturbation approximation holds when P is small. This condition is well fulfilled in the cases encountered in the present experiments (maximum value of $P \approx 1\,\%$). Another approximation made is that $N_{max} = 2$, i.e. we consider only one excited state. For the conditions encountered here it has been shown by accurate computer calculations that the influence of the higher-lying levels is indeed small.

In the perturbation expansion we can write

$$R \approx AB(\mathrm{E2}, 0^+ \rightarrow 2^+)[1.0 + \rho Q_{2^+}]. \tag{3}$$

The functions A and ρ depend on the charge number Z_i and mass number A_i of the projectile and target, (indices 1 and 2, respectively), on the bombarding energy E, on the scattering angle θ of the projectile, and on the excitation energy ΔE of the 2^+ state. The values of A and ρ for given bombarding conditions can be calculated with the help of the tables and formulae given in ref. [1]).

The quantity ρ represents the sensitivity of the measured quantity R on the quadrupole moment Q_{2+}. Since ρ is roughly proportional to A_1 it is advantageous to perform experiments with projectiles of large mass differences [1]).

2.3. COMPUTER EVALUATION

A computer program has been written [4]) which numerically solves the time-dependent Schroedinger equation in the semi-classical approximation. The program input consists of the relevant kinematical quantities and the target nucleus parameters. The latter include the energy level positions, spins, and E2 matrix elements M_{ik}. The matrix elements $M_{ik} = \langle k||\mathcal{M}(\mathrm{E2})||i\rangle$ are related to the $B(\mathrm{E2})$ values by

$$(M_{ik})^2 = B(\mathrm{E2}; I_i \rightarrow I_k)(2I_i+1) \tag{4}$$

and to Q_{2+} by

$$eQ_{2+} = -\tfrac{4}{5}(\tfrac{2}{7}\pi)^{\frac{1}{2}}M_{22} = -0.758M_{22}\,. \tag{5}$$

The output of the program, consisting of the cross sections, was used to calculate R_{comp} by formula (1).

By varying the input matrix elements M_{12} and M_{22} around values which are close to those giving the best fit to the experimental data, we can determine quantities A_{comp} and ρ_{comp} in such a way that

$$R_{\mathrm{comp}} \approx A_{\mathrm{comp}} B(\mathrm{E2}, 0^+ \rightarrow 2^+)[1.0+\rho_{\mathrm{comp}} Q_{2+}]. \tag{6}$$

The justification for writing R_{comp} in this form is the approximate validity of the perturbation expansion. Furthermore, computer calculations showed that in the expansion of R_{comp} quadratic and higher terms in Q_{2+} are negligible for the range of interest. It is the explicit dependence of R_{comp} on $B(\mathrm{E2}, 0^+ \rightarrow 2^+)$ and on Q_{2+}, given above, which was used in fitting the experimental data.

3. Experimental setup

3.1. BEAM PRODUCTION

The projectiles were accelerated by the Rutgers-Bell model FN Tandem Van de Graaff. The accelerator was operated with a maximum terminal voltage of 8.5 MV. The methods used to produce the various negative ion beams are given in table 1. For the ^{16}O beam, the evaporation of the BaO coating from the platinum mesh

filament provided a sufficient supply of oxygen in the duoplasmatron to permit the use of pure H_2 as the source gas.

TABLE 1
Production methods of negative ion beams

Negative ion	Duoplasmatron filament	Duoplasmatron gas	Exchange medium	Highest charge state accelerated	Max beam on target (nA)
^4He	coated Pt mesh	^4He	Li vapor	2^+	300
^{16}O	coated Pt mesh	H_2	H_2	6^+	400
^{32}S	Ta wire	10 % H_2S 90 % H_2	H_2	8^+	70

3.2. BEAM ENERGY DEFINITION

Due to the large variation of the excitation cross section with beam energy, it is necessary to have an accurate knowledge of the calibration of the analyzing magnet (90° magnet).

The absolute calibration of the magnet was performed using the $T = \frac{3}{2}$ resonance [5]) in $^{13}N^*$ which occurs at the proton laboratory energy of 14.233 ± 0.010 MeV. To check the linear dependence between the indication of the field measuring device and the momentum of the projectiles, the ratios of fields required to deflect $^4He^{1+}$ and $^4He^{2+}$ beams for a constant terminal voltage on the accelerator were measured. The results indicated that the linearity was preserved up to the high field values required to deflect the heavy ions.

3.3. MULTIPLE BEAMS

A complicating feature of heavy ion spectroscopy is that several projectiles can simultaneously be accelerated having approximately the same magnetic rigidity. It is therefore possible to have more than one type of projectile incident on the target at the same time. Since even small amounts of contaminating beams could affect the results of this experiment, an analysis of the incident beam was performed. This was accomplished by scattering the incident beam from a thin gold foil into a solid-state detector located at 20° with respect to the beam. Several peaks due to beams other than the primary one were generally found. However, after proper adjustments had been made to the focusing system of the accelerator, the intensities of the spurious beams could be kept at levels where their effect was negligible.

3.4. APPARATUS

A schematic view of the scattering chamber and the 20° monitoring system is shown in fig. 1. The defining aperture of the collimator system was a tantalum orifice of 1.5 mm diameter. The annular detector was placed 1.7 cm from the target,

which allowed particles to be accepted between the angles of 157° and 175°. The beveled NaI detector was positioned at 55° with respect to the beam with its front face 2.6 cm from the target.

Targets enriched to 95.7 % in ^{116}Sn and 94.7 % in ^{124}Sn were prepared by vacuum evaporation onto 5 or 10 μg/cm^2 carbon foils. The thickness of the targets ranged from 100 to 500 μg/cm^2.

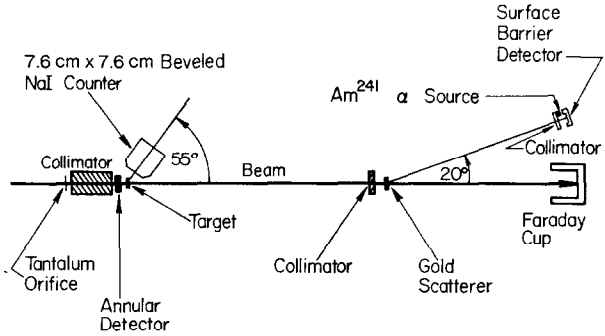

Fig. 1. Schematic view of the arrangement of the particle-gamma coincidence counters and the 20° scattering chamber used to measure the beam energy.

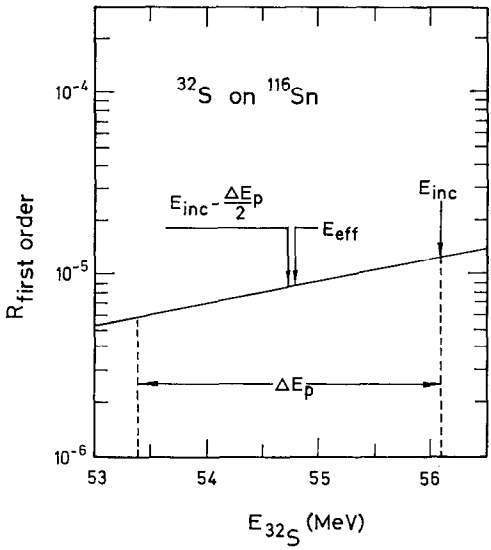

Fig. 2. Variation of the excitation probability P with bombarding energy E_p for a range of E_p corresponding to the energy loss ΔE_p of the beam in the target.

The annular Si-Au surface barrier detectors had active areas of about 150 mm^2 and depletion depths of 300 μm. The standard shape counters used for target thickness measurements were of the same type. The gamma counter was a 7.5 cm × 7.5 cm beveled NaI crystal coupled to an RCA 8054 photomultiplier.

3.5. EFFECTIVE BOMBARDING ENERGY

The quantity R is a very sensitive function of the bombarding energy. Fig. 2 shows a first order perturbation calculation of $R(E_p)$ covering the energy range from $E_{inc}-\Delta E_p$ to E_{inc} where ΔE_p is the energy loss in a typical target and E_{inc} is the incident bombarding energy. The effective bombarding energy E_{eff}, indicated in the figure, has been calculated by numerical integration of the cross section. The value of E_{eff} turns out to be very close to $E_{inc}-\frac{1}{2}\Delta E_p$. For the case of ^{32}S bombarding ^{116}Sn, a 0.1 % variation in E_{eff} changes R by 1.0 %. It is clear then that a rather careful determination of E_{eff} is necessary. The quantities entering the calculation of E_{eff} are E_{inc}, ΔE_p, and the stopping power dE/dx. The determination of the incident energy was discussed in subsect. 3.3.

Measurements of the target thicknesses were performed by scattering the beam by a thin gold foil into a solid state detector located at 20° with respect to the beam direction. (See fig. 1.) The resulting pulse height spectrum was recorded with the target in and out of the beam.

Several features complicated the target thickness measurement. It was found that the target thickness as obtained from the 20° monitor increased linearly with bombarding time. This was due to a build-up of "dirt" on the target. In the case of sulfur bombardment the change in target thickness caused by the build-up sometimes amounted to an energy loss of up to 700 keV. A series of measurements performed to determine the nature of the build-up revealed that it occurred only on the beam spot and that it was deposited in equal amounts on the front and back surfaces of the target. Using these results the actual target thickness was determined from the measurements made before the run. Furthermore, the calculation of the effective energy had to take into account the energy loss due to the build-up on the front of the target.

Since the stopping power of carbon is greater than tin, the energy lost by a heavy ion in the carbon backing may not be neglected. For example, a 60 MeV sulfur ion will lose about 200 keV in 10 $\mu g/cm^2$ of carbon. The thickness of each backing was determined by observing the scattering of 2 MeV α-particles [6]) into the annular detector. The values for the stopping power adopted for the calculation of the effective energy were extracted from our own measurements, Bichsel's work [7]) and the results of Booth and Grant [8]). It was found that for the target thicknesses encountered in this work the choice of stopping power is not too critical.

3.6. ELECTRONICS

The γ-ray spectrum was measured in coincidence with particles backscattered into the ring counter. Using a standard "fast-slow" coincidence circuit, a timing resolution of about 5 ns (FWHM) was obtained for γ-ray energies greater than 500 keV and particle energies corresponding to backscattering from tin. In practice, a timing window of 30 ns width was used to ensure 100 % coincidence efficiency. The gamma coincidence spectra were recorded in an SDS 910 computer, program-

med to store the true plus random spectrum in one 512-channel array, and the random spectrum in another.

4. Results

4.1. BACKSCATTERED PARTICLES

A spectrum of the backscattered particles is shown in fig. 3. The number of backscattered particles was determined by recording the number of pulses falling in an energy window set around the tin peak of the backscattered particle spectrum. Some of the spectra contained a high-energy background which was subtracted out. This correction was always less than 1.0 % of the total number of backscattered particles.

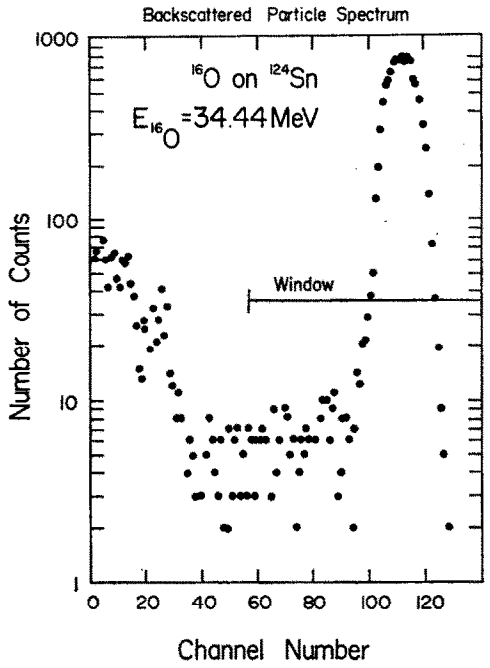

Fig. 3. Spectrum of backscattered particles.

The counting rate in the window was kept below 1000 counts/sec, thus making a correction for dead-time unnecessary. The use of a small beam intensity was also necessitated by the low melting point of tin.

The effect of the finite solid angle subtended by the annular particle detector can be accounted for by introducing an effective scattering angle θ_{eff}. Its determination is simplified considerably by realizing that the higher order terms in the cross section can be dropped in the averaging process without seriously affecting the value of θ_{eff}. The effective laboratory scattering angles encountered in the present experiments varied between 164° and 165°.

A correction to the γ-ray coincidence yield arises from the difference in the fraction of elastic and inelastic events in the low-energy tails that are cut off by the base line of the window. This correction amounted to almost 5 % in some cases.

4.2. GAMMA-RAY COINCIDENCE SPECTRA

The raw data acquired consisted of the number of particle detector pulses within the window and the gamma-ray coincidence spectrum, a sample of which is given in fig. 4.

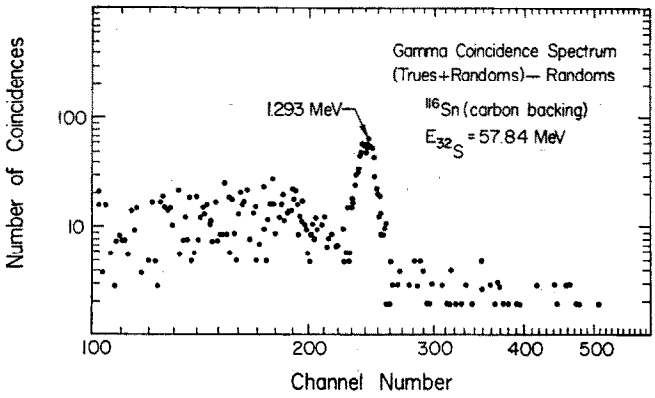

Fig. 4. Particle-gamma coincidence spectrum.

In the present series of experiments, the consistency of the data could be checked since each pair of projectiles yields an independent measurement of Q_{2+}. The data for the three projectiles (^{4}He, ^{16}O, ^{32}S) bombarding ^{116}Sn were found not to be consistent with a single value for Q_{2+}. In a previous preliminary communication [9]) the discrepancy was ascribed to the large errors of the experiment and to an interference term via a higher lying $2^{+\prime}$ state. Further experiments revealed that this interpretation was incorrect.

It was found that a 1265 keV γ-ray is produced when 35 MeV ^{16}O projectiles bombard the oxide impurity present on the target by the reaction:

$$^{16}\mathrm{O}+{}^{16}\mathrm{O} \rightarrow {}^{31}\mathrm{P}^{*}+\mathrm{p}$$
$$\hookrightarrow {}^{31}\mathrm{P}+\gamma\ (1265\ \mathrm{keV}).$$

The kinematics of this reaction is such that the backscattered protons have an energy of about 18 MeV. Although protons of this energy are not stopped in the detector, they were found to produce a high-energy tail in the particle spectrum reaching up to pulse heights accepted by the window. The probability of producing a 1265 keV γ-ray in coincidence with a backscattered proton was measured to be about 0.1. The probability of Coulomb exciting the 1293 keV level of ^{116}Sn with 35 MeV ^{16}O ions

is 0.001. The 1265 keV and the 1293 keV γ-rays are not resolved by the NaI detector. Therefore, if the intensity of the backscattered protons accepted by the particle window was only 0.1 % of the number of backscattered oxygen ions, the gamma intensity in the ^{16}O bombardment of ^{116}Sn would be increased by 10 % over the pure Coulomb excitation contribution. Since the precise amount of oxygen in the targets was not known, the oxygen data had to be ignored in the determination of the quadrupole moment of ^{116}Sn.

The quantity of interest, the number of 2^+ to 0^+ decays, was evaluated from the number of counts in the full-energy peak. Although the absolute peak intensities are evaluated, we are ultimately interested in the relative intensities of the full-energy peaks produced by different projectiles. Since the γ-ray spectra for different projectiles are similar, the relative intensities can be determined with higher precision than the absolute intensities.

An analysis utilizing the similarity of the spectra was achieved by plotting the spectra on a log-log scale. On this type of plot, spectra can be easily compared due to the fact that relative intensity and gain shifts can be accounted for by a parallel displacement of the spectra along the x- and y-axes. This method allowed account to be taken of the backgrounds under the full-energy peaks in a similar way in each spectrum.

In order to obtain absolute γ-ray intensities, the full energy peak efficiency of the NaI detector was determined by placing sources calibrated to ± 3 % at the target position. From this measurement the efficiencies of the 1.29 MeV ^{116}Sn line and the 1.13 MeV ^{124}Sn line were found to be 0.020 ± 0.001 and 0.022 ± 0.001, respectively.

4.3. GAMMA-RAY ANGULAR DISTRIBUTIONS

In order to normalize the γ-ray intensities to a 4π geometry, the anisotropy of the γ-ray angular distribution must be accounted for. The angular distribution for the geometry of this experiment is given by

$$W(\theta_\gamma) = 1 + a_2^{(2)} A_2^{(2)} (J_2/J_0) P_2(\cos\theta_\gamma) + a_4^{(2)} A_4^{(2)} (J_4/J_0) P_4(\cos\theta_\gamma).$$

The angle between the symmetry axis of the gamma detector and the beam direction is denoted by θ_γ. The quantities $a_2^{(2)}$ and $a_4^{(2)}$ have been calculated by the computer code [4]).

The angular correlation coefficients $A_2^{(2)}$ and $A_4^{(2)}$ are 0.3571 and 1.143, respectively. The geometrical attenuation coefficients J_2/J_0 and J_4/J_0 defined by Rose [11]) were measured for the beveled crystal used in this experiment and were found to have values of 0.773 and 0.379, respectively, for the 1.29 MeV ^{116}Sn line, and 0.769 and 0.374, respectively, for the 1.13 MeV ^{124}Sn line. The 2nd and 4th order Legendre polynomials are denoted by P_2 and P_4. The value of $W(\theta_\gamma)$ varied between 1.19 and 1.23 for the various projectiles and energies used in this experiment. The following corrections to the γ-ray angular distribution have been considered:

(i) The effect due to the solid angle subtended by the particle detector. This has been accounted for by integrating the $a_2^{(2)}$ and $a_4^{(2)}$ coefficients (which are functions of the particle scattering angle) weighted by $d\sigma_2$ over the detector solid angle.

(ii) The alteration of the γ-ray angular distributions due to the velocity of the recoil target nucleus, as described in ref. [1]). This adds extra terms to eq. (7). In the cases considered here, the correction is less than 1 %.

(iii) The attenuation of the angular distribution from magnetic deorientation. Simpson and Smilansky [12]) have pointed out that the γ-ray angular distribution may be attenuated due to the highly ionized state of the target recoiling into the vacuum. The dependence of the attenuation on the lifetime of the recoil nucleus has been studied by Ben Zvi *et al.* [13]). They find the attenuation coefficients are given by

$$G_K = (1 + C_K \tau)^{-1},$$

where τ is the lifetime of the nuclear state and C_K is a factor depending upon the nature of the interaction. The coefficients C_K have been measured [14]) for ^{114}Cd (τ = 9 ps). Assuming the same values of C_K for the Sn isotopes (τ = 0.4 and 0.8 ps) we find that the attenuation effects are negligible in our experiments.

4.4. EXPERIMENTAL DATA

The experimental results are summarized in tables 2 and 3 for ^{116}Sn and ^{124}Sn, respectively. The errors quoted are the errors for relative intensities. The absolute efficiency has an uncertainty of about 5 %.

TABLE 2

Experimental data for ^{116}Sn

Projectile	E_p (MeV)	R_{exp} ($\times 10^{-4}$)	% error
^{4}He	9.952	4.21	5.5
	11.176	11.55	4.0
	11.881	16.60	3.6
^{32}S	54.788	1.14	12
	57.312	2.06	5.1
	58.083	2.69	6.5
	68.485	19.81	5.0

TABLE 3

Experimental data for ^{124}Sn

Projectile	E_p (MeV)	R_{exp} ($\times 10^{-4}$)	% error
^{4}He	9.970	5.96	3.1
^{16}O	34.435	18.67	4.0
	35.030	22.87	4.7
	41.860	92.75	3.6
^{32}S	54.797	2.86	12
	57.276	4.63	5.7
	57.787	5.06	4.3

5. Analysis and interpretation

5.1. ANALYSIS BY COMPUTER PROGRAM

For the analysis of the data a set of computer runs has been performed for each measurement listed in tables 2 and 3, and the coefficients A_{comp} and ρ_{comp} [see eq. (6)] were determined for each case. The sensitivities ρ_{comp} were then corrected for quantal effects using the curves given in ref. [15]).

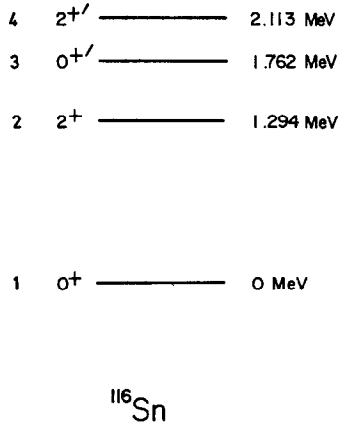

Fig. 5. Energy level diagram of ^{116}Sn, showing those levels which were included in the computer analysis.

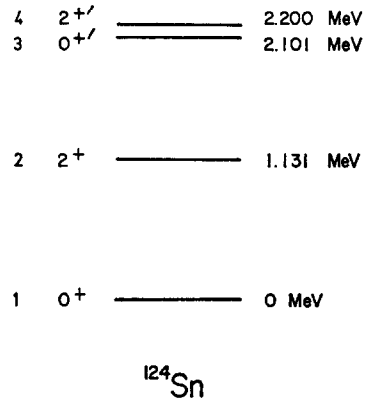

Fig. 6. Energy level diagram of ^{124}Sn, showing those levels which were included in the computer analysis.

The energy levels included in the computer analysis are given in figs. 5 and 6 for ^{116}Sn and ^{124}Sn, respectively. The spins of the levels above the first 2^+ state in ^{124}Sn have not been measured and were assigned on the basis of systematics of neighboring nuclei. The input E2 matrix elements connecting levels above the first 2^+ state are given in table 4. For ^{116}Sn these matrix elements were obtained from the branching and mixing ratio measurements [16]) of the $2^{+\prime} \rightarrow 2^+$ and $2^{+\prime} \rightarrow 0^+$ transitions, and from comparison with matrix elements in ^{114}Cd. For ^{124}Sn all matrix elements were obtained by a comparison with ^{116}Sn.

TABLE 4

E2 matrix elements $M_{ik} = \langle k||\mathcal{M}(\mathrm{E2})||i\rangle$ in ^{116,124}Sn in units of $e^2 \cdot b^2$

Isotope	M_{14}	M_{23}	M_{24}
^{116}Sn	0.05	−0.17	−0.50
^{124}Sn	0.05	−0.16	−0.47

The quantities M_{12} and M_{22} were fitted to the data. Two computer runs with either sign of M_{12} were performed to study the contribution of the interference term via the $2^{+\prime}$ state. The indices refer to the level schemes in figs. 5 and 6.

Since the spins of ^{124}Sn and the matrix elements of the higher levels for both ^{116}Sn and ^{124}Sn are uncertain, it is important to know their effect on the evaluation of the measured quantities in terms of the quadrupole moment of the excited state.

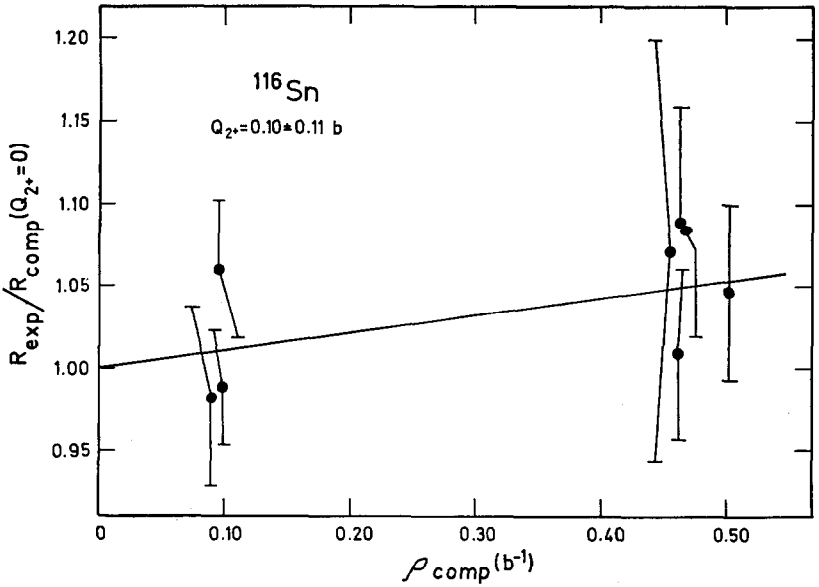

Fig. 7. Fit of the experimental data for ^{116}Sn to the computer results, for the choice of a positive sign for the interference term. The slope of the fitted straight line is equal to the static quadrupole moment.

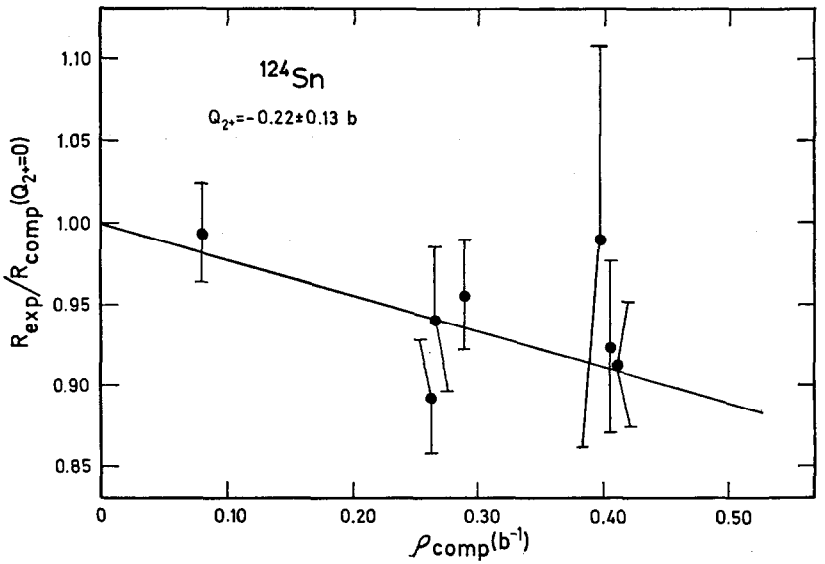

Fig. 8. Fit of the experimental data for ^{124}Sn to the computer results, for the choice of a positive sign for the interference term. The slope of the fitted straight line is equal to the static quadrupole moment.

This has been examined by varying the relevant quantities for several computer runs. The largest and only non-negligible effect arising from the higher levels is due to the unknown sign of the interference term involving the second 2^+ state as an intermediate state.

The data has been plotted in figs. 7 and 8 in the following way: The ordinate shows

$$\frac{R_{\text{exp}}}{R_{\text{comp}}(Q_{2^+} = 0)} = \frac{R_{\text{exp}}}{B(\text{E2})A_{\text{comp}}}. \tag{9}$$

The sensitivity of R to the value of the static moment Q_{2^+} given by ρ_{comp} is plotted on the abscissa. A straight line is then fitted to the points. The input $B(\text{E2}, 0^+ \rightarrow 2^+)$ value to the computer program has been adjusted to give an intercept of 1.0 with the ordinate. The slope of the fitted line determines the value of Q_{2^+}.

TABLE 5
Experimental results

Isotope	Sign of interference term	Q_{2^+} (b)	$B(\text{E2}, 0^+ \rightarrow 2^+)$ $(e \cdot \text{b})^2$	$\frac{1}{5}\chi^2$
^{116}Sn	+	$+0.10 \pm 0.11$	0.223 ± 0.013	0.61
	−	$+0.07 \pm 0.11$	0.222 ± 0.013	0.59
^{124}Sn	+	-0.22 ± 0.13	0.188 ± 0.013	0.59
	−	-0.25 ± 0.14	0.188 ± 0.013	0.57

The results of the fits are listed in table 5. The $B(\text{E2})$ values found for both nuclei are in good agreement with the measurements of Stelson *et al.* [17]). The chi-square values for the quality of the fits obtained for either choice of the sign of the interference term $\langle 0^+ || \mathcal{M}(\text{E2}) || 2^+ \rangle \langle 0^+ \mathcal{M}(\text{E2}) || 2^{+\prime} \rangle \langle 2^{+\prime} || \mathcal{M}(\text{E2}) || 2^+ \rangle$ do not allow us to make the choice between the two possible signs.

Calculations based on quasiparticle theories [2,3]) give $B(\text{E2})$ values for both isotopes which are a factor of 2 to 4 smaller than the experimental values. The theoretical calculations for Q_{2^+} all fall within the rather large limits of error for ^{116}Sn. However, our value of $Q_{2^+}(^{124}\text{Sn})$ has the opposite sign of those calculated in ref. [2]).

The authors wish to thank Hans P. Lie of Bell Telephone Laboratories for his valuable advice and assistance during all phases of this work.

References

1) J. de Boer and J. Eichler in Advances in nuclear physics 1, eds. M. Baranger and E. Vogt (Plenum Press, N.Y., 1968) p. 1
2) P. L. Ottaviani, M. Savoia and J. Sawicki, Nuovo Cim. **56B** (1968) 149
3) M. Gmitro, A. Rimini, J. Sawicki and T. Weber, Phys. Rev. Lett. **20** (1968) 1185

4) A. Winther and J. de Boer, A computer program for multiple Coulomb excitation, reprinted in K. Alder and A. Winther, Coulomb excitation (Academic Press, New York and London, 1966)
5) D. Bredin, O. Hansen, G. Temmer and R. Van Bree, in Isobaric spin in nuclear physics, eds. J. D. Fox and D. Robson (Academic Press, N.Y., 1966) p. 472
6) R. Hill, Phys. Rev. **90** (1953) 845
7) H. Bichsel, in AIP Handbook, 2nd ed. (1963)
8) W. Booth and I. S. Grant, Nucl. Phys. **63** (1965) 481
9) A. M. Kleinfeld, R. Covello-Moro, J. de Boer and H. P. Lie, Bull. Am. Phys. Soc. **12** (1967) 564
10) R. Keddy and Y. Yoshizawa, Nucl. Phys. **85** (1966) 537
11) M. Rose, Phys. Rev. **91** (1953) 610
12) J. J. Simpson and U. Smilansky, Phys. Lett. **26B** (1968) 581
13) I. Ben-Zvi, P. Gilad, M. Goldberg, G. Goldring, A. Schwarzschild, A. Sprinzak and Z. Vager, Nucl. Phys. **A121** (1968) 592
14) J. D. Rogers, J. Gastebois, A. M. Kleinfeld, S. G. Steadman and J. de Boer, Bull. Am. Phys. Soc. **14** (1969) 122
15) K. Alder and H. K. A. Pauli, Nucl. Phys. **A128** (1969) 193
16) H. H. Bolotin, Phys. Rev. **136** (1964) 1557
17) P. H. Stelson, F. K. McGowan, R. L. Robinson, W. T. Milner and R. O. Sayer, Phys. Rev. **170** (1968) 1172